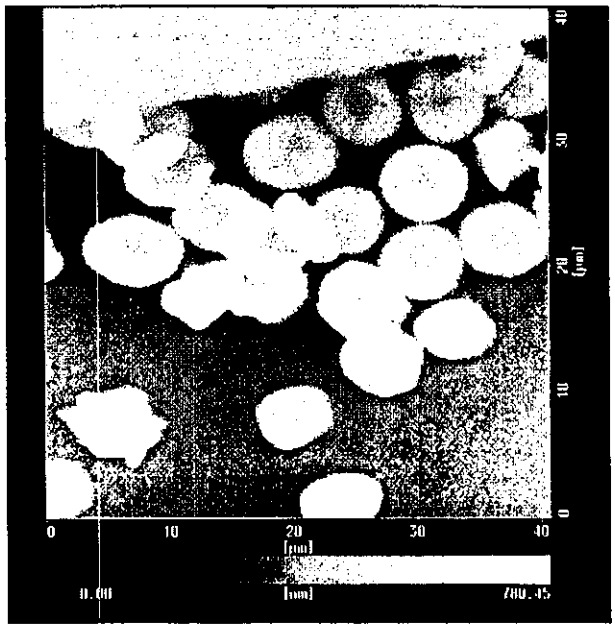

図5　羊保存血液の軟X線像
X軸Y軸ともにフルスケールで40 μm。図の下部のX線像の高さを表すカラーバー表示の最大値は，780 nm

板上で培養した神経細胞を，グルタルアルデヒド固定とt−ブチルアルコール法により凍結乾燥した試料を用いた。現在使用している軟X線顕微鏡では，試料ホルダーに試料を入れてX線露光装置にセットするまで1分程度は必要で，この間に環境変化に敏感な神経細胞は形成していた成長円錐を引っ込めてしまう。このため，生かしたままでは成長円錐の観察は困難であった。したがって上記のようにまず固定操作を行った。神経細胞はサイズが大きいため，図6にはX線像の一部を示した。細胞体から突起が伸び出して拡がっている様子がわかる。よく知られている扇形の広がりとは異なった形状に見受けられるが，培養に用いたPMMAは通常使用されている合成樹脂の培養ディッシュやガラスとは異なる素材であるため，神経細胞の成長のしかたが異なっていた可能性やグルタルアルデヒド固定の間に成長円錐が萎縮した可能性が考えられる。X線像を更に拡大した図6(b)では，ミトコンドリアと見られる構造が見られる。

水中での観察例として，細胞分裂中のクラミドモナスの観察例を図7に示した[11]。クラミドモナスは緑藻類に属する単細胞生物で葉緑体を持ち，光合成をするとともに2本の鞭毛を持ち水中を泳ぎまわることができる。植物であるため細胞壁を持っている。栄養条件がよいと細胞分裂により無性生殖を行う。図7に示したX線像に特徴的なことは，最外側の分裂前の細胞（母細胞）の細胞壁が見られ，その内側で分裂している娘細胞の周りに新しい細胞壁が形成されている様子が見受けられることである。クラミドモナスの細胞壁の外側は多糖類の層で覆われていると考えられている。図7に見られる娘細胞の周りの幅広い細胞壁は，水を豊富に含んだ構造体である。

水を多量に含んだゲル状の構造は，乾燥処理によって萎縮してしまうが，軟X線顕微鏡のように水中での観察ができると，炭素密度の低

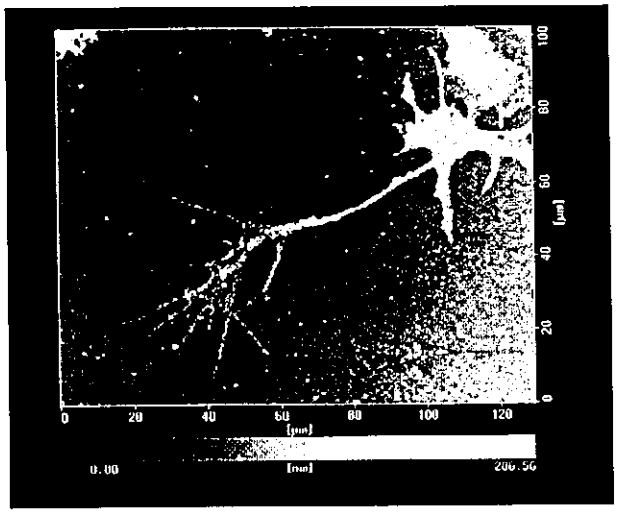

図6(a) PMMA上で培養したニワトリ胚の後根神経節のX線像

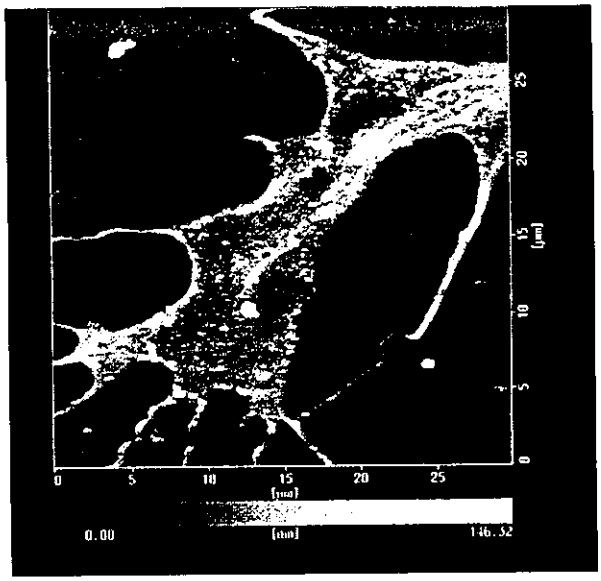

図6(b) 図6(a)の部分拡大図
＊ミトコンドリア

い構造として画像化される。図8にクラミドモナスのX線像の細胞壁周辺を拡大した像を示した。細胞体の外側に炭素濃度の低い構造があることがわかる。このように，炭素密度分布を画像化できる軟X線顕微鏡観察は，多糖類を潤沢に含む細胞外マトリックスなど電子顕微鏡の適用が困難な水中で発達している壊れやすい構造を高分解能で可視化する方法として期待で

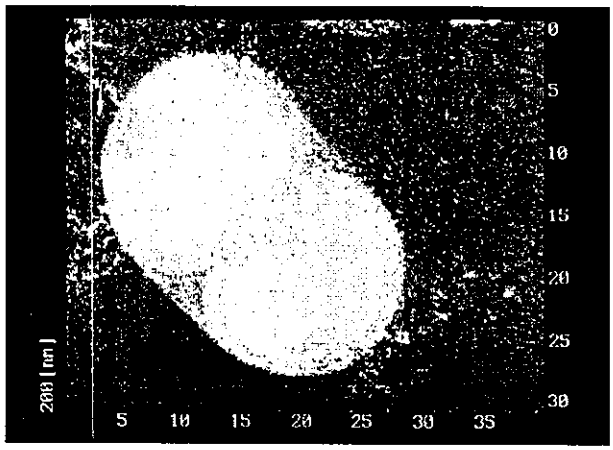

図7　細胞分裂中の緑藻類クラミドモナス

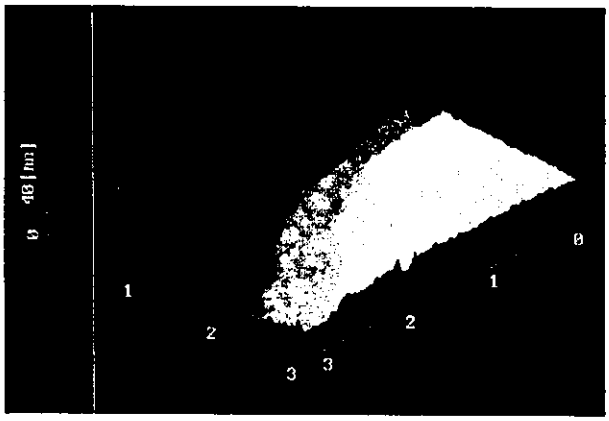

図8　緑藻類クラミドモナスの細胞壁周辺の拡大X線像，XY軸のスケールは3 μm，図の右側が細胞体，左側が培地部分

きる。

4. 密着型X線顕微鏡法の応用例

レーザプラズマ軟X線源によるX線顕微鏡法を，中性子捕捉療法（Neutron Capture Therapy：NCT）と呼ばれる放射線がん治療法における細胞内線量分布測定法に応用した例を紹介する[7,8]。

NCTは，中性子捕獲断面積の大きい核種を含む化合物に腫瘍集積性を持たせ，外部から照射される少量の熱中性子との核反応で生ずる放射線を用いて腫瘍細胞にダメージを与える新しいタイプの放射線治療法である。NCTでは主に^{10}B化合物が用いられホウ素中性子捕捉療法（BNCT）と呼ばれ，世界各国の臨床試行で良好な治療成績を収めている。BNCTの特徴は，^{10}B(n, α)^{7}Li反応で生じるα線及びLi反跳核の飛程が細胞1個分程度（～10 μm）であり，

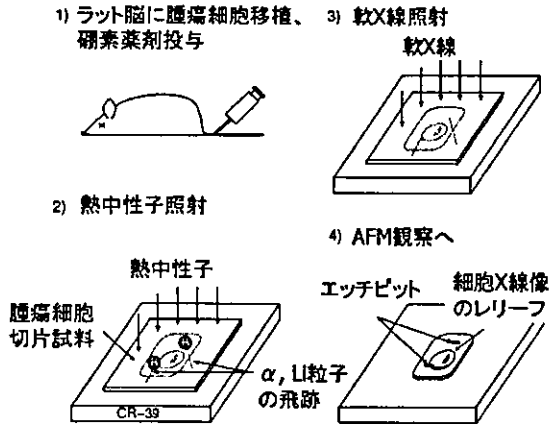

図9 細胞内ホウ素分布測定手法の概念図

放射線エネルギーの全てを細胞1個の範囲内に落とすため殺細胞性が極めて高いことである。また，ホウ素薬剤が腫瘍細胞のみに集積していれば，隣接する正常細胞を傷つけることなく腫瘍のみを選択的に撃退できる。浸潤の激しい腫瘍（悪性脳腫瘍・悪性黒色腫等）を患部の機能を温存したまま根治できる画期的な治療法である。

BNCTのキーポイントは，(1)理想的な熱・熱外スペクトルを有する強力中性子源開発と，(2) ホウ素薬剤の腫瘍選択性と取込量向上，が挙げられる。(2) については，BSH及びBPAと呼ばれる腫瘍集積性ホウ素化合物が見出されているが，更に十分に集積比・取込量を上げるべくホウ素薬剤の化学修飾や新規ホウ素薬剤の開発が盛んに行われている。しかし，その取り込み機構は必ずしも解明されておらず，それを調べるための細胞内微小器官のレベルでのホウ素薬剤の分布測定法自体も開発途上の段階にある。

そこで各種ホウ素薬剤によるBNCTの治療効果の評価やホウ素薬剤の輸送メカニズムの解明に資するデータを取得する目的で，ホウ素分布測定法のひとつである中性子誘起αオートラジオグラフィー法に密着型軟X線顕微鏡法を組み合わせ，詳細な細胞構造イメージ中にホウ素分布をマッピングする手法を開発した。具体的には図9に示すように，ホウ素－中性子反応により発生したα線やLi反跳核のトラックとともに，軟X線暴露により細胞の“影絵”をプラスチックポリマー上に記録，同時観察する手法であるが，これを高分解能化し細胞内微小器官のスケールで観察できるようにした。

記録用ポリマーにはCR-39プラスチック飛跡検出器を用いた。CR-39は短時間のアルカリエッチングにより微小なα線のトラック（エッチピット）を生成するので，これをAFMを用いて高分解能観察する方法である（図10）。CR-39はレーザプラズマ軟X線に対しても感度を有し，100 nmの分解能で軟X線像を記録できることを見出した。図11はCR-39の一部をマスクした状態でレーザプラズマ軟X線を照射し，高温の水酸化ナトリウム溶液でエッチングした際に，CR-39表面に現れた段差のプロファイルをAFMで観察したものである。

図12は，担癌ラットにホウ素薬剤を投与し，2時間後にがん組織を取り出してエポン包埋切片とし，CR-39にマウントして図9の手順で実

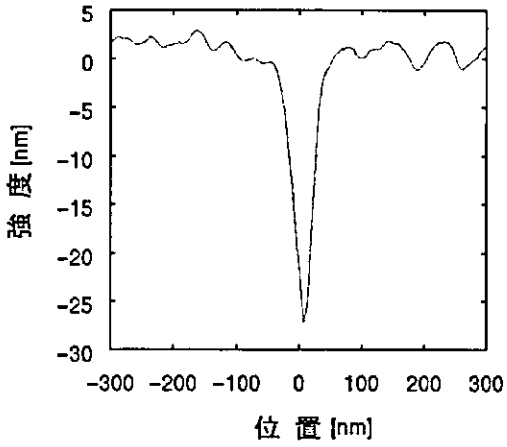

図 10　CR-39 プラスチック飛跡検出器表面に生じた微小 α 線トラック（エッチピット）の断面図（AFM 観察による）

際に細胞内ホウ素分布（α 線トラック発生分布）を測定したものである。細胞像は細胞核，細胞質及び間質の部分が明確に区別できていることがわかる。α 線トラックのエッチピットは 100 nm 級の分解能で観察できており，細胞内構造レベルでの分布測定が可能である。

BNCT における α オートラジオグラフィー法は，単にホウ素分布を定量的に測定するにとどまらず，実際に中性子を照射した際の電離性荷電粒子の発生分布も調べることができる。バックグラウンドとして発生するプロトンも検出できるから，治療時の線量分布も同時に計測できる。しかし，これを細胞内微小器官のスケールで測定する工夫はこれまで皆無であった。細胞内の放射線感受性は，細胞核（感受性高）と核外（感受性低）とで大きく異なる上，荷電粒子線は飛跡に沿って極めて狭い範囲に高密度な損傷をもたらす性質がある。このため，細胞内での α 線・Li 粒子の発生分布は，BNCT の治療効果を判定する上で薬剤の腫瘍選択性にも増して重要な情報である。本手法は，ポリマー上に記録された飛跡（エッチピット）及び細胞透過像のレリーフを AFM で高分解能観察することで細胞内微小器官スケールでの観察を可能にする。この手法により，BNCT で急務とされる新規ホウ素薬剤開発のためのホウ素薬剤の詳細な局在情報が得られるものと考えられる。

BNCT における細胞内ホウ素分布測定法としては，α オートラジオグラフィー法のほか，ホウ素化合物の抗体を用いた免疫染色法及び二次イオン質量分析法（SIMS）による元素分布

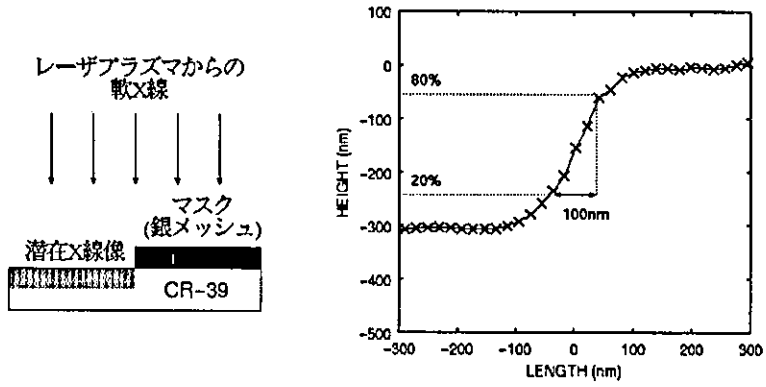

図 11　CR-39 を用いたレーザプラズマによる軟 X 線顕微鏡の解像度測定実験の概略と結果
エッチング後の CR-39 表面に生じた段差のエッジ広がりは約 100 nm で，これが分解能となる

図 12(a) ホウ素薬剤の細胞内分布測定結果の例（AFM 像）
矢印は α 線トラックのエッチピットを示す。スケールバー 5 μm

図 12(b) 同一試料の低倍像
エッチピットは白色の点として見やすく拡大表示してある。スケールバーは 10 μm

マッピングが主流である。しかし現状の方法では，細胞内構造まで画像化するには難がある，固定・染色などの処理をする場合に水溶性ホウ素薬剤が溶出する可能性がある，などの問題を抱えている。本研究で提案する手法は，AFMによる高分解能観察に加え，細胞イメージングに密着型軟X線顕微鏡法を用いるので，固定・染色を必要としないことから，国内外のBNCTコミュニティでもその価値が認められつつある。BNCTに携わる医師や製薬研究者との協力研究も始められた。

5. その他のX線顕微鏡

X線顕微鏡は，まだ開発途上の装置であるがその歴史は古い[9]。1895年にレントゲンによりX線が発見されて間もなく，X線の持つ高い物質透過性を活かしたX線顕微鏡の作製が試みられたが，X線を結像させることが当時の技術ではできなかった。写真乾板上に直接試料を置いて露光する方法も試みられたが，乾板の分解能が粗く，顕微鏡レベルで期待される微細構造の観察はできなかった。1940年代になると結像型のX線顕微鏡が実現されたが，光学顕微鏡の分解能を超えることはできなかった。一方，1897年にブラウン管が発明されて以降，電子線の利用技術が発展し1933年には電子顕微鏡が登場し，生物試料に限らず微細構造の高分解能観察手段として現在に至るまで幅広く利用されている。X線顕微鏡が再び注目を集めるようになったのは，集積回路の開発が進みリソグラフィー技術を中心とする微細加工技術などX線顕微鏡に関連する周辺技術が発展した1980年代以降である。

現在使われているX線顕微鏡は，密着型X線顕微鏡，結像型X線顕微鏡，投影型X線顕微鏡，走査型X線顕微鏡に大別される。密着型X線顕微鏡は，既に述べたようにX線感光材料の上に直接に試料を密着させておき，試料の実物大のX線像を得る装置である。

結像型X線顕微鏡は，X線ミラーやフレネルゾーンプレートなどのX線光学素子を用いてX線を結像させ，X線像を得るものである[10]。X線像の拡大を行うので，検出器自体の分解能は必ずしも高い必要はなく，写真フィルムあるいはマイクロチャネルプレート，CCDカメラなどを用いることができるのが利点である。問題点は，ゾーンプレートなどの作製に高精度の微細加工技術が必要とされる点である。

また，密着型X線顕微鏡と比べて拡大X線像が得られるメリットはあるが，作製できるゾーンプレートの大きさが限られているため，画像形成に必要なX線露光を長時間行う必要があるので，生きている生物試料の観察に用いるには制限が大きい。しかしながら，波長選択性が高い放射光を用いると，蛍光X線を観察して生体内の微量元素の分析やその分布を画像化するなど，蛍光X線顕微鏡として利用できる。ホヤの赤血球に含まれるバナジウムの分布を観察した報告がある[11]。放射光の持つ高い波長選択性を活用した蛍光X線顕微鏡は，微量元素の分析機器として生体試料の観察以外にも考古学分野への応用など幅広い活用が期待できる。

投影型X線顕微鏡は，点X線源とスクリーンとの間に試料をおき，試料の投影拡大像を得る。電子線を金属薄膜に照射し点X線源とするものが電子顕微鏡を改造して作製され，昆虫や蚤などの内部構造が観察されている[12),13)]。

走査型X線顕微鏡は，試料を走査させながらX線ビームを照射するもので，試料の微小部分からの情報を得ることができる。

6. おわりに

本稿では，レーザー生成プラズマをX線源に用いた密着型フラッシュ軟X線顕微鏡の原理と応用例について解説した。この装置は水中にある試料の高分解能観察ができるので，培養細胞などを生理的条件下で観測することができる。特にゲル状の構造体など，電子顕微鏡や光学顕微鏡では観察が困難なものを高分解能で観察できる利点は大きい。またコロイドなど，水

の中での状態を観察することに本質的な意味がある対象を観察できることも利点である[14]。

軟X線顕微鏡法を中性子捕捉療法における細胞内線量分布測定法に応用した例で述べたように，PMMA以外のX線感光材料をX線像の記録媒体に用いることも可能である。今後，細胞診断などさまざまな用途への応用が期待できる。

謝　辞

密着型フラッシュ軟X線顕微鏡の研究開発は，産業技術総合研究所の前身である電子技術総合研究所の複数の研究部に所属する背景の異なる研究者の学際的な協力により行われたものである。腫瘍の中性子補足療法における細胞内線量分布測定法への応用は，複数の大学・病院・研究機関に所属する研究者の学際的な協力により行われたものである。多くの関係者の方々に謝意を表したい。また密着型フラッシュ軟X線顕微鏡の研究の一部は，平成14年度以降「厚生労働科学研究費補助金（萌芽的先端医療技術推進研究事業）」により行われた。

文　献

1) Majima, T., Shimizu, H., Tomie, T., Miura, E., Kanayama, T. and Yamada, M., X-ray imaging of living cells, *Proc. SPIE*, 2983, 81-88 (1997)
2) Majima, T., Shimizu, H. and Tomie, T., Recent advances in soft x-ray microscopy for living specimens, *Bioimages*, 7, 59-67 (1999)
3) Shimizu, H., Tomie, T., Majima, T., Stead, A. D., Ford, T. W., Miura, E., Yamada, M. and Kanayama, T., X-ray Microscopy and Spectroscopy, (Thieme, J., Schmahl, G., Rudolph, D. and Umbach, E. eds.), pp.I-157-162, Springer-Verlag, Berlin (1998)
4) 眞島利和，X線顕微鏡による生体の計測，現代化学，386，51-55 (2003)
5) Tomie, T., Shimizu, H., Majima, T., Yamada, M., Kanayama, T., Kondo, H., Yano, M. and Ono, M., Three-dimensiomal readout of flash X-ray images of living sperm in water, *Science*, 252, 691-693 (1991)
6) Schneider, G., Niemann, B., Guttmann, P., Rudolph, D. and Schmahl, G., Cryo X-ray microscopy, *Synchrotron Radiation News*, 8, 19-28 (1995)
7) Amemiya, K., Takahashi, H., Nakazawa, M., Shimizu, H., Majima, T., Nakagawa, Y., Yasuda, N., Yamamoto, M., Kageji, T., Nakaichi, M., Hasegawa, T., Kobayashi, T., Sakurai, Y. and Ogura, K., Soft x-ray imaging using CR-39 plastics with AFM readout, *Nucl. Instrum. Methods Phys. Re., Sect. B*, 187, 361-366 (2002)
8) 雨宮邦招，成瀬　徹，高橋浩之，中沢正治，中川義信，清水秀明，眞島利和，安田仲宏，山本幹男，櫻井良憲，古林　徹，CR-39とAFMを用いたBNCTマイクロドシメトリ，放射線，27，55-59 (2001)
9) Kirtz, J., Jacobsen, C. and Howells, M., Soft X-ray Microscopes and Their Biological Applications, *Qurt. Rev. Biophys.*, 28, 33-130 (1995)
10) 渡岡　武，山下広順　共編，X線結像光学，培風館 (1999)
11) 木原　裕，竹本邦子，X線顕微鏡の応用，電子顕微鏡，39，8-12 (2003)
12) Yoshimura, H., Maeda, H., Hori, A., Horikoshi, T., Takata, H. and Igarashi, K., *J. Phys. IV France*, 104, 355-358, (2003)
13) Yoshimura, H., Application of the Projection X-ray Microscopy to Biological Specimen, *Proc. Arthropod Embryol. Soc. Jpn.*, 38, 1-8 (2003)
14) Furusawa, K., Matsumura, H. and Majima, T., Characterization of silica-coated hematite and application to the formation of composite particles including egg yolk PC liposomes, *J. Col. Int. Sci.*, 264, 95-100 (2003)

COMMUNICATION

ChemComm
www.rsc.org/chemcomm

Patterning of DNA nanostructures on silicon surface by electron beam lithography of self-assembled monolayer

Guo-Jun Zhang,*[a] Takashi Tanii,[b] Takashi Funatsu[ac] and Iwao Ohdomari[abd]

[a] *Nanotechnology Research Center, Waseda University, Waseda Tsurumaki-cho 513, Shinjuku-ku, Tokyo 162-0041, Japan. E-mail: zhang@kaw.comm.waseda.ac.jp; Fax: +81-3-5286-9076; Tel: +81-3-5286-9067*

[b] *Department of Electronical Engineering and Bioscience, School of Science and Engineering, Waseda University, 3-4-1 Okubo, Shinjuku-ku, Tokyo 169-8555, Japan*

[c] *Department of Physics, School of Science and Engineering, Waseda University, 3-4-1 Okubo, Shinjuku-ku, Tokyo 169-8555, Japan*

[d] *Kagami Memorial Laboratory for Materials Science and Technology, Waseda University, 2-8-26 Nishi-waseda, Shinjuku-ku, Tokyo 169-0051, Japan*

Received (in Cambridge, UK) 25th November 2003, Accepted 16th February 2004
First published as an Advance Article on the web 5th March 2004

Nanoscale patterns of modified oligonucleotides are produced on octadecyltrimethoxysilane self-assembled monolayers at a silicon surface by electron beam lithography. DNA structures with feature sizes of the order of 250 nm were detected by epi-fluorescence microscopy.

DNA chips have been widely used as high-throughput screening assays to identify genetic variations associated with disease for discovery of new drugs.[1,2] Conventional patterning techniques, such as spot arraying[3] and photolithography,[4] have been employed to fabricate DNA arrays at sizes ranging from tens to hundreds of microns. The miniaturization of feature sizes and the spatially controlled immobilization of biomolecules on these miniaturized features on the nanometre scale become more important, mainly due to further requirements including increased density of biochip components, reduced amount and volume of a sample, and higher detection sensitivity. Therefore, arrays with smaller features lead to the development of DNA nanochips with faster analysis speed and massive parallelization.

Dip-pen nanolithography is well known for its ability to directly pattern DNA nanostructures on the metal and insulator surfaces.[5] However, it is difficult to achieve a high spatial precision since the size of the DNA pattern primarily relies on the fabrication speed and a humid environment. An atomic force microscopy (AFM) based lithography technique known as nanografting was also used to produce nanostructure of DNA on a gold surface.[6] This method offers a high spatial precision but has the limitation of low throughput. Self-assembled monolayers (SAMs) have been developed for high resolution nanofabrication techniques because of their potential use as an ultra-thin resist layer and capability of resisting the non-specific binding of biomolecules.[7] Electron beam (EB) lithography is a commonly used nanofabrication means and does not need direct substrate contact and has advantages over scanned probe lithography technique when nanostructures are patterned on SAM.

Recently, we demonstrated the immobilization of DNA on microstructured patterns fabricated by EB lithography using a conventional resist.[8] However, there is a demand for a thin electron-beam resist in the future of nanometre scale lithography because this resist deposited on SiO_2 is too thick to achieve high resolution nanofabrication. In addition, since 3-aminopropyltriethoxysilane (APTES) is a small molecule and does not form oriented self-assembled monolayers, it actually forms multilayers packed inside the amino-modified micropatterns. As soon as the resist was removed, some of the APTES molecules on the top of the multilayer were laid down onto the SiO_2 surface around the patterns, thereby leading to irregular fluorescence pattern expansion. Therefore, it is impossible to use this method to further fabricate DNA nanopatterns. In this work, we introduce a new method to produce DNA nanostructures on octadecyltrimethoxysilane (ODS) SAM at a silicon surface using EB lithography. The use of ODS SAM enables us to miniaturize the feature sizes and obtain a high signal-to-noise ratio. We also demonstrate that these DNA nanostructures can be produced with almost no detectable non-specific binding of DNA in the regions outside nanopatterns.

As illustrated in Fig. 1, the approach described here includes several steps: fabrication of nanometre-sized patterns by EB lithography of ODS SAM at a silicon surface followed by site-directed immobilization of oligonucleotides onto these nanopatterns and subsequent hybridization of fluorescently labeled target to immobilized DNA within those nanopatterns.

ODS SAM, formed through chemical bonding of molecules to the oxidized silicon substrates, can be used as an ultrathin resist for EB lithography, and a passivation layer for preventing non-specific adsorption of biomolecules as well. Typically, an ODS monolayer is deposited on SiO_2 surfaces by immersing the substrates into a solution containing ODS.[7] However, this method frequently leads to microstructural defects such as aggregates or holes at the surfaces.[9] Clearly, such inhomogeneous surfaces cannot serve as ideal templates for biomolecule modification and may cause difficulties in the characterization of subsequently assembled layers. Although the formation of ODS SAM onto cleaned SiO_2 substrates by chemical vapor deposition (CVD) has been described elsewhere,[10] nothing is known about the conditions of ODS SAM by CVD for nanofabrication using EB lithography. In this experiment, the parameters of CVD for the formation of ODS SAM of high quality were optimized. Briefly, an ODS monolayer was deposited on a SiO_2 layer at 110 °C for 3 h under N_2 by CVD and the surface was washed with chloroform for 10 min by ultrasonication. The thickness of the ODS monolayer estimated from AFM imaging is ~2.0 nm. The resulting ODS monolayer is homogeneous with low roughness and terminated with methyl groups, leading to the minimization of biomolecular adhesion.

After fabrication of the nanopatterns, the sample is immersed in a solution of 3-aminopropyltriethoxysilane (APTES) for modifying the nanodot areas with an amine group terminated APTES layer. Clearly, APTES is a smaller molecule than ODS. However, the ODS monolayer contains many pinholes, indicating that APTES can easily be deposited in the pinhole areas between two ODS molecules, resulting in a strong background outside the patterned regions. In this work, after the silicon substrate was modified with an ODS monolayer, another small molecule, ethyltriethoxysilane (ETS), was introduced to prevent APTES assembly in the pinhole

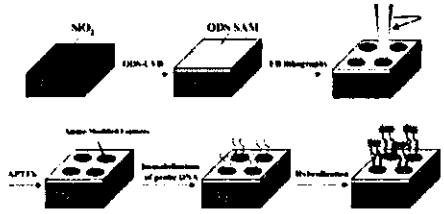

Fig. 1

DOI: 10.1039/b315278b

areas by filling up the pinholes prior to fabrication of nanopatterns by EB lithography. The surface covered with an ODS monolayer was immersed in a solution of 1 mM ETS in ethanol for 1 h. After washing with ethanol by ultrasonication, the monolayer was exposed to a dose of 960 μC cm^{-2} at 20 keV using an electron beam. All patterning was done with an electron beam lithography system (Hitachi S-4200, Japan). The patterned surface was developed using buffered hydrofluoric acid (BHF) for 60 s; subsequently, the nanopatterns on the ODS monolayer developed.

Patterns after nanofabrication by EB lithography on the ODS monolayer were imaged by tapping-mode AFM (Fig. 2). The dark dots correspond to the patterned regions. Fig. 2a shows regular submicron-sized patterns, in which the distance between the two dots is 5 μm and the diameter of the dots is 500 nm. Smaller nanopatterns are shown in Fig. 2b, in which the distance and the diameter are 2.5 μm and 250 nm, respectively. The measured depth of each dot is ~3 nm, indicating that the electron beam has penetrated through the ODS monolayer and the patterned regions were exposed with the SiO_2 surface.

To immobilize amine-modified oligonucleotides onto the nanopatterns generated by EB lithography of ODS monolayer, a typical approach using APTES and glutaraldehyde as bifunctional cross-linkers was employed according to our previous protocol.[8] Two types of sequences both complementary and non-complementary were applied to this experiment: H_2N-5′-$(T)_{15}$-CCACGGAC-TACTTCAAAACTA-3′ (complementary probe), H_2N-5′-ATC-GATCGATCGATCGATCGA-3′ (non-complementary probe). Noticeably, a fragment of extra sequence (T_{15}) in the complementary probe was designated to introduce a long spacer (the predicted length of the fully stretched fragment is ~6 nm) between the complementary sequence and the surface because it will be able to minimize steric hindrance, increase the corresponding hybridization efficiency and thereby improve the detection sensitivity. To demonstrate the sequence specificity, patterned oligonucleotides, both complementary and non-complementary, were exposed to a solution containing a fluorescently labeled target whose sequence is: Cy 5–5′- TAGTTTTGAAGTAGTCCGTGG-3′. The patterned regions were incubated with a 1 μM Cy 5 labeled target in 2 × SSC, 0.2% Tween-20 (v/v) at 59 °C for 2 h. The patterns were then characterized by epi-fluorescence microscopy (Fig. 3). Fig. 3a–c exhibited low background, demonstrating that very little non-specific binding of biomolecules on the ODS SAM is detected. On the contrary, DNA nanostructures with dot arrays (500 nm dots, 5 μm pitch and 250 nm dots, 2.5 μm pitch) were strongly visualized in Fig. 3a and 3b, respectively. Owing to DNA–DNA interaction, homogeneous patterns of the hybridization of a target labeled with Cy 5 to the complementary probe were observed with strong fluorescence signals within the nanoscale patterns (Fig. 3a and 3b). However, as shown in Fig. 3a and 3b, some of the spots appeared brighter than the rest mainly due to unequal amounts of DNA attachment. On the other hand, in the case of non-complementary probe DNA, no fluorescence patterns could be seen because of

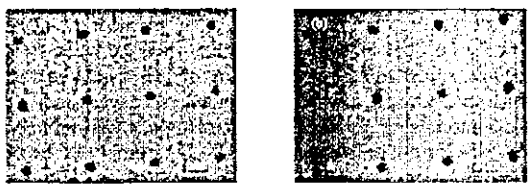

Fig. 2 Tapping mode AFM images showing nanodots after nanofabrication on ODS SAM by EB lithography: (a) dot size: 500 nm, pitch: 5 μm; (b) dot size: 250 nm, pitch: 2.5 μm.

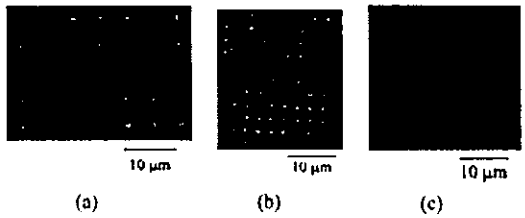

Fig. 3 Fluorescence micrographs of Cy 5 labeled target hybridized to probe DNA immobilized within nanodot areas fabricated by EB lithography on ODS SAM at a silicon surface: (a) complementary probe DNA (spot size: 500 nm, spacing: 5 μm); (b) complementary probe DNA (spot size: 250 nm, spacing: 2.5 μm); (c) non-complementary probe DNA.

unspecific binding between non-complementary sequence and target (Fig. 3c). These data indicate that probe DNA was preferentially immobilized on patterned regions of the surface and confirm the specificity of binding between the target and immobilized probe DNA.

In conclusion, this work demonstrates a novel approach for patterning DNA nanostructures on a silicon substrate based on EB lithography of ODS SAM. Through nanofabrication using EB lithography on ODS monolayers deposited on a silicon dioxide surface by CVD, nanostructures capable of being chemically modified can be generated. As a result, these nanostructures can be functionalized with amine-modified oligonucleotides, which maintain their hybridization specificity toward the complement. The procedures described here provide a protocol for creating well-defined DNA nanostructures on substrates, which will find increased applications in the field of DNA biosensors and biochips. However, sub-100 nm nanopatterns are difficult to detect by fluorescence microscopy due to the resolution limitations of the optical technique. Further work is under way to visualize several or tens of nano-scale DNA patterns by other techniques.

We thank Ms Mikiko Saito of the Nanotechnology Foundry at Waseda University for assistance with the AFM experiments. This work is supported in part by the Japan Society for the Promotion of Science (JSPS), and a Grant-in-Aid for Center of Excellence (COE) Research from the Ministry of Education, Culture, Sports, Science and Technology.

Notes and references

1 E. S. Lander, *Nat. Genet.*, 1999, **21**, 3.
2 T. R. Golub, D. K. Slonim, P. Tamayo, C. Huard, M. Gaasenbeek, J. P. Mesirov, H. Coller, M. L. Loh, J. R. Downing, M. A. Caligiuri, C. D. Bloomfield and E. S. Lander, *Science*, 1999, **286**, 531.
3 M. Schena, D. Shalon, R. W. Davis and P. O. Brown, *Science*, 1995, **270**, 467.
4 S. P. A. Fodor, J. L. Read, M. C. Pirrung, L. Stryer, L. A. Tsai and D. Solas, *Science*, 1991, **251**, 767.
5 (*a*) L. M. Demers, D. S. Ginger, S.-J. Park, Z. Li, S.-W. Chung and C. A. Mirkin, *Science*, 2002, **296**, 1836; (*b*) H. Zhang, Z. Li and C. A. Mirkin, *Adv. Mater.*, 2002, **14**, 1472.
6 M. Liu, N. A. Amro, C. S. Chow and G.-Y. Liu, *Nano Lett.*, 2002, **2**(8), 863.
7 (*a*) C. S. Whelan, M. J. Lercel, H. G. Craighead, K. Seshadri and D. L. Allara, *Appl. Phys. Lett.*, 1996, **69**, 4245; (*b*) M. J. Lercel, H. G. Craighead, A. N. Parikh, K. Seshadri and D. L. Allara, *Appl. Phys. Lett.*, 1996, **68**, 1504.
8 G.-J. Zhang, T. Tanii, T. Zako, T. Funatsu and I. Ohdomari, *Sens. Actuators B*, 2004, **97**(2–3), 243.
9 D. F. S. Petri, G. Wenz, P. Schunk and T. Schimmel, *Langmuir*, 1999, **15**, 4520.
10 K. Hayashi, N. Saito, H. Sugimura, O. Takai and N. Nakagiri, *Langmuir*, 2002, **18**, 7469.

Molecular Cell, Vol. 14, 423–434, May 21, 2004, Copyright ©2004 by Cell Press

GroEL Mediates Protein Folding with a Two Successive Timer Mechanism

Taro Ueno,[1,4] Hideki Taguchi,[2,3,4,5] Hisashi Tadakuma,[1] Masasuke Yoshida,[2,*] and Takashi Funatsu[1,*]
[1]Department of Physics
School of Science and Engineering
Waseda University
3-4-1 Okubo
Tokyo 169-8555
[2]Chemical Resources Laboratory
Tokyo Institute of Technology
4259 Nagatsuta
Yokohama 226-8503
[3]Precursory Research for Embryonic Science and Technology (PRESTO)
JST
Kawaguchi-shi, Saitama 332-0012
Japan

Summary

GroEL encapsulates nonnative substrate proteins in a central cavity capped by GroES, providing a safe folding cage. Conventional models assume that a single timer lasting ~8 s governs the ATP hydrolysis-driven GroEL chaperonin cycle. We examine single molecule imaging of GFP folding within the cavity, binding release dynamics of GroEL-GroES, ensemble measurements of GroEL/substrate FRET, and the initial kinetics of GroEL ATPase activity. We conclude that the cycle consists of two successive timers of ~3 s and ~5 s duration. During the first timer, GroEL is bound to ATP, substrate protein, and GroES. When the first timer ends, the substrate protein is released into the central cavity and folding begins. ATP hydrolysis and phosphate release immediately follow this transition. ADP, GroES, and substrate depart GroEL after the second timer is complete. This mechanism explains how GroES binding to a GroEL-substrate complex encapsulates the substrate rather than allowing it to escape into solution.

Introduction

In prokaryotes and eukaryotes, chaperonins facilitate folding of newly translated, newly translocated, or stress-damaged proteins in an ATP-dependent manner. The best-studied of these chaperonins is the *Escherichia coli* GroEL and its cochaperonin GroES (Bukau and Horwich, 1998; Sigler et al., 1998; Thirumalai and Lorimer, 2001; Hartl and Hayer-Hartl, 2002; Saibil and Ranson, 2002). GroEL comprises 14 identical 57 kDa subunits each containing a site for binding and hydrolysis of ATP (Braig et al., 1994; Boisvert et al., 1996). Seven GroEL subunits are arranged in a heptamer ring forming a central cavity, and two heptamer rings are stacked back to back (Braig et al., 1994). GroES is a dome-shaped, single heptamer ring of 10 kDa subunits (Hunt et al., 1996; Xu et al., 1997).

GroEL binds a wide range of nonnative proteins at the apical cavity rim (Viitanen et al., 1992; Horwich et al., 1993; Fenton et al., 1994; Ewalt et al., 1997; Houry et al., 1999), then subsequently binds ATP and GroES to the same (*cis*) GroEL ring (Xu et al., 1997), producing the *cis* ternary complex consisting of GroEL, nonnative protein, and GroES (Weissman et al., 1995; Mayhew et al., 1996). Since the residues of GroEL involved in GroES binding mostly overlap with those responsible for substrate protein binding (Fenton et al., 1994), it is presumed that, when GroES binds to GroEL, residues within GroES assume responsibility for binding from substrate protein. Then, instead of escaping into the bulk medium, nonnative protein is somehow guided into the cavity of the *cis* ring beneath GroES (the *cis* cavity) where it can initiate folding without risk of aggregation (Fenton et al., 1994; Xu et al., 1997; Chen and Sigler, 1999). As ATPs in the *cis* ring are hydrolyzed to ADP, the opposite side (*trans*) ring of GroEL becomes ready for binding nonnative proteins and ATP, which, in turn, induces the release of GroES, ADP, and substrate protein (whether folded or not) from the *cis* ring (Rye et al., 1997, 1999). Then the *trans* ring subsequently binds GroES, becoming a new *cis* ternary complex for the next chaperonin cycle (Rye et al., 1997, 1999). The functional GroEL cycle proceeds at maximum turnover rate, ~0.12 s^{-1}, when saturating amounts of GroES, ATP, and nonnative proteins are present (Burston et al., 1995; Rye et al., 1999). Under these optimum conditions, binding of these components to GroEL is very rapid, and, according to current model, the whole cycle of GroEL is actually governed by a single rate constant (0.12 s^{-1}) corresponding to the rate of ATP hydrolysis in the *cis* ring (the single timer model) (Weissman et al., 1996; Rye et al., 1997, 1999). Therefore, when the cycle is initiated by addition of ATP to the mixture of GroEL, substrate protein, and GroES, the folding-active *cis* ternary complex should form immediately and all subsequent events, including those of ATP hydrolysis reactions (cleavage of bound ATP, release of ADP and Pi) and decay of the *cis* ternary complex (release of GroES and substrate protein from GroEL), should take place apparently with a single rate constant, ~0.12 s^{-1}. As a result, the substrate protein can utilize almost the whole functional GroEL cycle of ~8 s [lifetime, 1/(0.12 s^{-1})] for productive folding.

However, single molecule imaging of dynamic binding release kinetics of GroES during steady-state functional GroEL cycle has revealed that release of GroES from GroEL occurs through two steps defined by rate constants, ~0.3 s^{-1} and ~0.2 s^{-1} (Taguchi et al., 2001). Typically, GroES binds very rapidly to GroEL, remains for ~3 s (lag period), and departs GroEL over ~5 s (Taguchi et al., 2001). Similar "two timer" kinetics of the

*Correspondence: myoshida@res.titech.ac.jp (M.Y.); funatsu@mol.f.u-tokyo.ac.jp (T.F.)
[4]These authors contributed equally to this work.
[5]Present address: Department of Integrated Biosciences, Graduate School of Frontier Sciences, The University of Tokyo, Kashiwa, Chiba 277-8562, Japan.

release of GroES from GroEL were observed by rapid scanning atomic force microscopy (Viani et al., 2000). These observations are in contrast to the prediction by the single timer model. This is not a trivial contradiction of kinetics because the appearance of another rate constant means the existence of a previously unnoticed intermediate in the functional GroEL cycle that would considerably improve our understanding on the GroEL mechanism. Indeed, a mutant GroEL that did not fit any of the intermediates in the single timer model has been reported (Kawata et al., 1999; Miyazaki et al., 2002).

Despite of a number of reports on GroEL kinetics, there is very little data which might distinguish the single timer model and the two timer model. Here, we report results on the kinetics of the functional GroEL cycle in the presence of ATP, GroES, and nonnative substrate proteins. For this purpose, we have developed a real-time, single molecule observation system for folding of green fluorescent protein (GFP) in the *cis* cavity and found that protein folding started after a lag period of ~3 s. Rearrangements of substrate protein in the *cis* cavity on this time scale were observed for GFP and malate dehydrogenase (MDH) by fluorescence resonance energy transfer (FRET). A second kinetic step necessitated the formation of new intermediates in the functional GroEL cycle, and initial pre-steady-state ATPase kinetics further clarified nucleotide states of these intermediates. This two timer mechanism may provide a possible explanation for the difficult problem of how GroEL can confine a substrate protein within the narrow *cis* cavity.

Results

Single Molecule Imaging Revealed that GFP Folding Was Arrested for the First ~3 s in the *cis* Ternary Complex

To analyze the events in a functional GroEL cycle, we need to monitor the recovery of the activity of the substrate protein in the *cis* cavity as a mark of completion of folding, with a time resolution of s, rather than min. Many studies on the time courses of GroEL(GroES)-mediated protein folding have been published, but few have reported such measurements. The substrate protein for this purpose should exhibit monomer activity that can be measured continuously while it is confined in the *cis* cavity. Since GFP exclusively satisfies these criteria, we developed a real-time, single molecule imaging system to observe folding of GFP in the *cis* cavity (Figure 1A). To immobilize and visualize GroEL, Asp490, which is located at the external surface of GroEL, was replaced by Cys (the mutant was termed EL490) and labeled with biotin-maleimide and IC5-maleimide at the same time. Labeled EL490, as well as unlabeled EL490, behaves like the wild-type GroEL as assessed by every analysis performed, including steady-state ATP hydrolysis and assisted folding of rhodanese and GFP as described previously (Taguchi et al., 2001). In addition, the second mutation D398A was introduced to EL490, termed EL398/490. Like a D398A mutant of GroEL, EL398/490 forms a *cis* ternary complex normally, but it hydrolyzes ATP very slowly, only 2% of wild-type (Rye et al., 1997). In the absence of ATP hydrolysis, EL398/490 keeps GFP in the *cis* cavity up to ~30 min where GFP can complete folding. GFP was denatured in 0.1 M HCl and diluted into a solution of neutral pH containing EL398/490 to form the EL398/490-GFP complex. The complex was infused into a flow cell and immobilized on the glass surface through biotin-streptavidin linker. The glass chamber was then filled with the solution containing GroES and caged ATP. First, the positions of EL398/490 molecules were determined by the fluorescence of IC5 using a total internal reflection fluorescence microscopy (TIRFM) (Figure 1B, "GroEL"). The functional GroEL cycle was triggered by generation of ATP from caged ATP (1 mM) on UV flash. About 40% of caged ATP was converted to ATP. As concentrations of generated ATP and GroES (1 μM) were saturating, their binding to GroEL should not limit the rate but should complete within 0.1 s, as calculated from the binding rate constants and concentrations (Taguchi et al., 2001). Following the photogeneration of ATP, fluorescent spots of the folded GFP appeared over time at the positions of EL398/490 (Figure 1B, "GFP"). Fluorescent spots of GFP that appeared at positions other than preassigned GroEL ones were ascribed to EL398/490 without the IC5 label. Folded GFP in the medium, if any, was not detected due to Brownian motion. All fluorescent spots were of the folded GFP within the *cis* ternary complex since no spots appeared in the absence of GroES.

A histogram of the waiting time for the appearance of GFP fluorescence showed a nonexponential distribution with a maximum at ~8 s (Figure 1C). The same data was replotted as the time course of the accumulated number of fluorescent GFP after UV flash (Figure 1C, inset) to compare with those of the following bulk phase experiments (Figure 2). The data shown in Figure 1C is well described by Equation 1 containing two transitions:

$$\text{denatured GFP}^* \xrightarrow[k]{} \text{denatured GFP} \xrightarrow[k']{} \text{native GFP} \quad (1)$$

A simulation of Equation 1 was plotted in Figure 1C with $k = 0.31\ s^{-1}$ and $k' = 0.034\ s^{-1}$ and, therefore, the lifetimes (the reciprocal of the rate constant) of "denatured GFP*" and "denatured GFP" were ~3 and ~33 s, respectively. This means that folding of GFP is arrested during the first ~3 s after GroES binds GroEL.

To avoid argument that these features are specific for the ATPase-deficient mutant, similar experiments were also performed using EL490. EL490 undergoes the normal functional GroEL cycle, and most GFP should be released into the bulk medium before folding is completed. Therefore, to keep maximum GFP in the *cis* cavity during the measuring time, we included apyrase in the reaction mixture to exhaust ATP within ~1 s after the UV flash so that the release of GroES from GroEL was suppressed by the lack of ATP for binding the *trans* ring (Rye et al., 1997, 1999). A histogram of the waiting time for the appearance of GFP fluorescence at the positions of EL490 after photogeneration of ATP showed a nonexponential distribution with a maximum at ~5 s (Figure 1D). The pattern of this histogram differed significantly from that of EL398/490. We measured the time course of the GroES release in the presence of apyrase using Cy3-GroES in a parallel experiment under the same conditions and calibrated the original data, taking into ac-

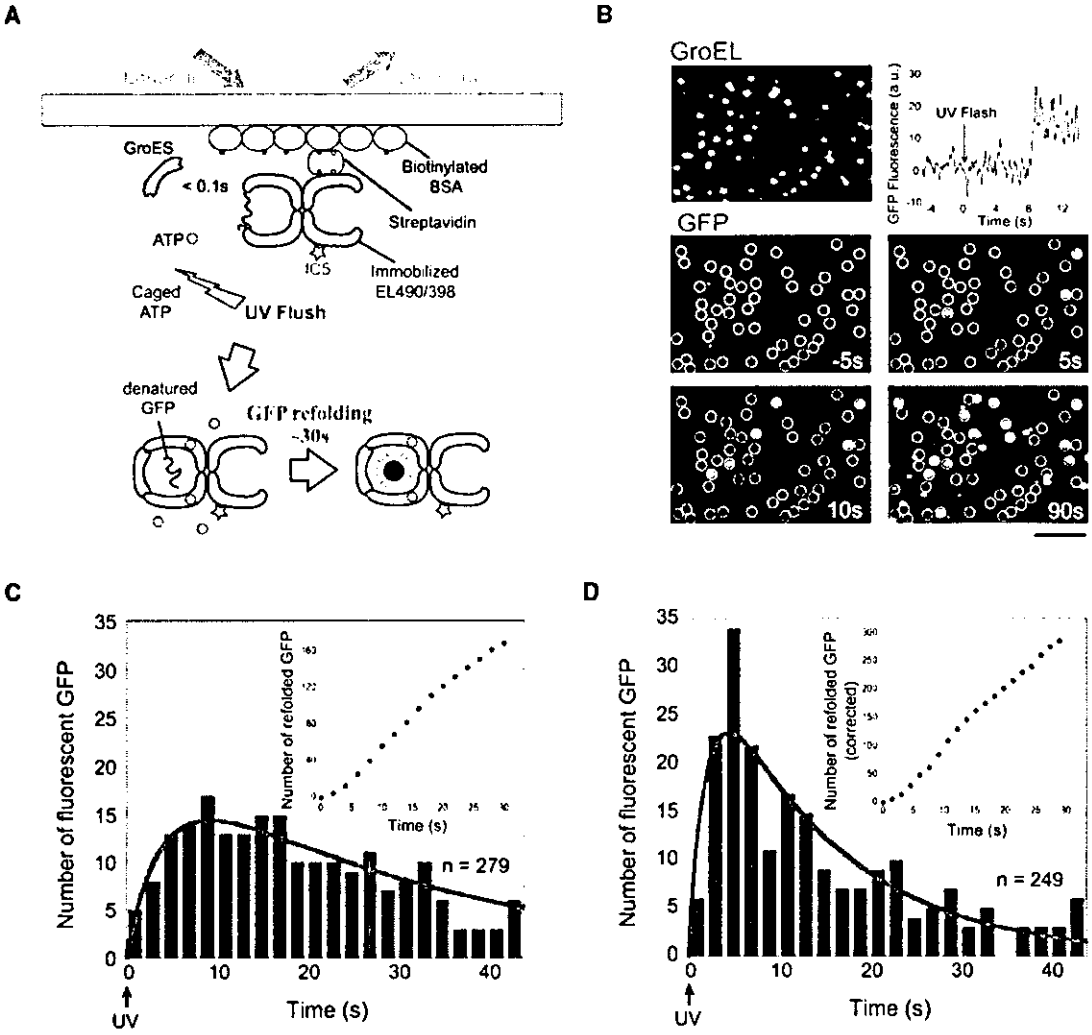

Figure 1. Imaging of Folding of Single Molecule GFP in the *cis* Cavity

(A) Schematic illustration of the experiment. The IC5-GroEL-denatured GFP complex was immobilized on the glass, and ATP was generated from caged ATP by a UV flash in the presence of a saturating amount of GroES. Appearance of GFP at the positions of GroEL was observed with TIRFM.

(B) Fluorescence images of GroEL molecules (GroEL) and GFP molecules (GFP), which folded within the *cis* cavity. ATP was generated at time 0 s. Positions of EL398/490 were indicated by circles colored yellow. Scale bar, 5 μm. (Inset) Time course of the fluorescence intensity of a GFP molecule at the position of GroEL (see Supplemental Movie S1 at http://www.molecule.org/cgi/content/full/14/4/423/DC1).

(C and D) Histograms of the time required for each GFP to gain native structure in (C) EL398/490 or (D) EL490, after the photogeneration of ATP. The solid line is the convolution of two exponentials, $Ck\,k'\,[\exp(-kt) - \exp(-k't)]/(k - k')$, fit to the data by least-squares fitting. This formula is derived from the two-step reaction of Equation 1. (Inset) Time course of the cumulative number of folded GFP molecules. Solid line is the integration of the above formula.

count the premature release of GFP. Including this correction, the histogram fit the two sequential transitions of Equation 1 with $k = 0.34\ s^{-1}$ and $k' = 0.029\ s^{-1}$ (gray line). The result again indicates that folding of denatured GFP in the *cis* ternary complex is arrested for ~3 s before it begins to regain the native conformation in the course of ~30 s. If the lag of ~3 s comes not from substrate release but from the kinetics of GFP refolding after release, the data in Figures 1 and 2 would be the remarkable evidence that the kinetics of protein refolding in the chaperonin cavity is completely different from those in free solution.

Bulk Phase Experiments Also Showed a ~3 s Lag of GFP Folding in the *cis* Ternary Complex

GFP folding was also monitored in bulk phase solution using a fluorometer (Figure 2A). Spontaneous folding, initiated by diluting acid-denatured GFP into a buffer of neutral pH, occurred with a single rate constant $0.032\ s^{-1}$. In this case, no lag was evident (Figure 2B). For GroEL-mediated GFP folding, acid-denatured GFP was diluted to a buffer containing GroEL and GroES to form the GroEL-GFP complex, and the functional GroEL cycle was initiated by addition of ATP. We tested three types of GroEL: EL490, EL398, and a single ring version

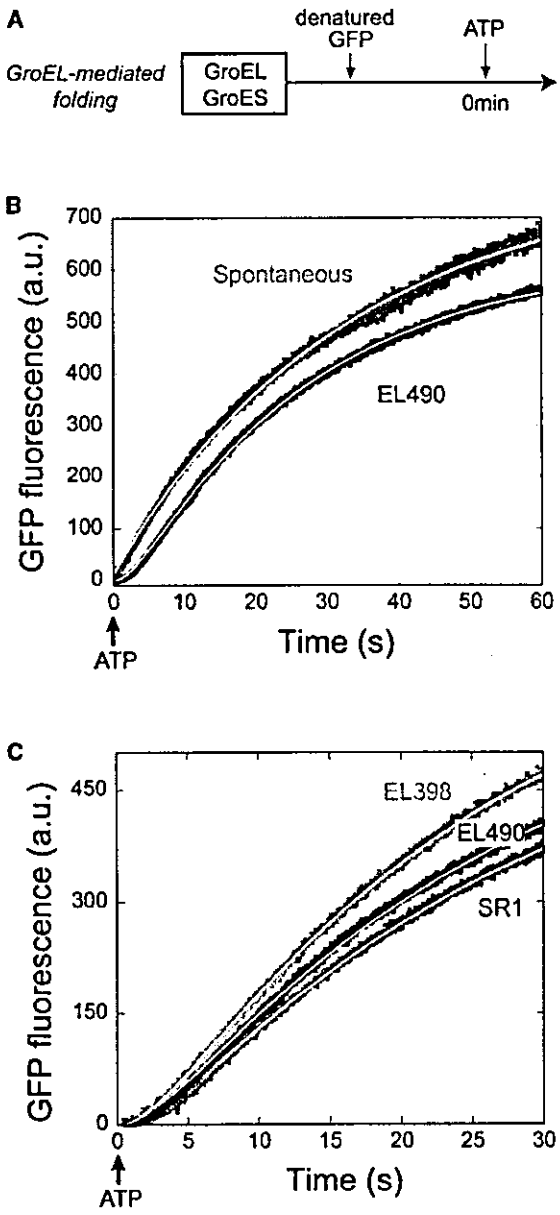

Figure 2. Bulk Phase Measurement of GFP Folding

(A) Diagram of experiments. GFP folding was initiated by adding ATP at 0 s to a buffer A containing GroES and the EL490-denatured GFP complex. Spontaneous folding of GFP was initiated by diluting acid-denatured GFP into buffer A.

(B) Spontaneous GFP folding and GFP folding in the presence of EL490. Spontaneous folding was fit by a single exponential. GFP folding in the presence of EL490 is fit to the data by the convolution of two exponentials.

(C) GFP folding in the presence of EL490, EL398, or SR1.

of GroEL (SR1) (Weissman et al., 1995). In the latter two cases, GFP was not released to the medium but remained in the *cis* cavity due to deficient ATPase (EL398) or lack of the signal from the *trans* ring (SR1). For every GroEL tested, folding of GFP started with an initial lag (Figures 2B and 2C). The time courses were well simulated by Equation 1, and rate constants of GFP folding mediated by EL490, EL398, and SR1 were obtained as k = 0.35, 0.35, and 0.30 s^{-1} and k' = 0.038, 0.040, and 0.037 s^{-1}, respectively. Simulated lines are shown by solid lines in Figure 2B. Thus, folding kinetics in the bulk phase experiments were very similar to those observed by single molecule imaging. A comment should be added that the results with SR1 appear to exclude the involvement of the *trans* ring in the initial kinetics of GFP folding.

Lags in GFP Folding and GroES Release Varied in the Same Way at Different Temperatures

We previously demonstrated single molecule imaging of binding-release dynamics of GroEL-GroES complex in the functional GroEL cycle (Taguchi et al., 2001). Analysis showed that, without added nonnative protein, release of GroES from GroEL occurred very slowly, but with added nonnative protein, GroES left GroEL in several seconds through two successive steps (Equation 2).

$$[\text{ES-EL}]^* \underset{k}{\rightarrow} [\text{ES-EL}] \underset{k'}{\rightarrow} [\text{ES}] + [\text{EL}] \qquad (2)$$

Very similar rate constants were obtained for four kinds of nonnative substrate proteins. These were k = 0.26–0.34 s^{-1} and k' = 0.18–0.24 s^{-1}, that is, GroES remains bound to GroEL for ~3 s and then leaves GroEL in ~5 s, independent of species of nonnative protein. These values were not affected by GroES concentrations in the medium (Taguchi et al., 2001). Since the ~3 s lag coincided with that of GFP folding, we postulated that it probably reflected the same transition of the *cis* ternary complex.

To confirm this, we examined whether the lag in GroES release and GFP folding varied in the same way at different temperatures. Single molecule imaging of GroES binding and release was carried out as described (Taguchi et al., 2001) (Figure 3A). To supply nonnative protein during the observation period, pepsin, a permanently denatured protein at neutral pH (Aoki et al., 1997), was used as a substrate protein. Because GroES release kinetics are largely unaffected by the species of nonnative protein (Taguchi et al., 2001), we compared the kinetics of GroES release in the presence of pepsin to those of GFP folding. Binding and release of individual Cy3-ES molecules to IC5-EL490 were visualized by TIRFM at 18°C, 23°C, and 28°C. Histograms of the duration of bound state (on time) were simulated by Equation 2. The first rate constants (k) were 0.19, 0.33, and 0.44 s^{-1}, and the second rate constants (k') were 0.086, 0.14, and 0.21 s^{-1} at 18°C, 23°C, and 28°C, respectively (Figure 3B). The values increased in parallel with temperature. GFP folding was observed by single molecule imaging with ATPase-deficient EL398 and with EL490 under single turnover conditions by ATP quenching with apyrase. Bulk phase GFP folding also was measured. Plots of rate constants corresponding to the initial lags of GroES-release kinetics and those of GFP folding clearly showed that the values agreed fairly well at all three temperatures (Figure 3C). These results indicate that lag of GroES release and the lag of GFP folding reflects the same transition in the *cis* ternary complex.

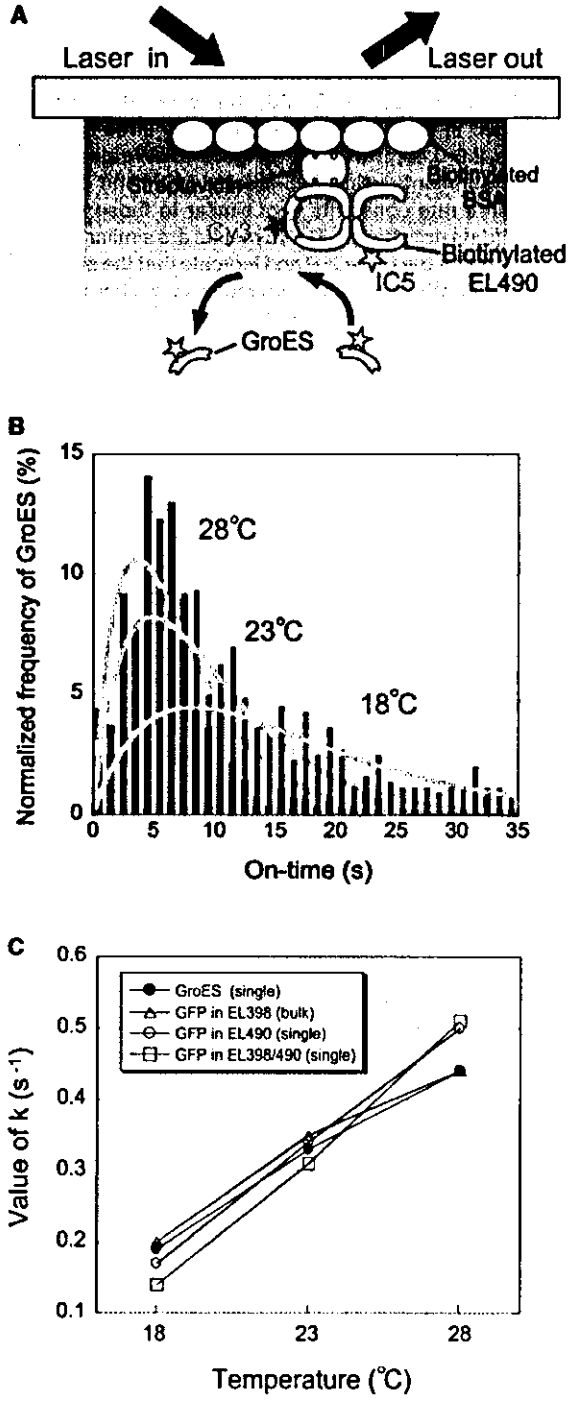

Figure 3. Temperature Dependency of the Lag Period of GFP Folding and that of GroES Release

(A) Schematic illustration of the single molecule imaging of the GroEL-GroES dynamics. Cy3-GroES was seen as a spot only when it bound to EL490 ("on time").

(B) Histograms of duration of GroES on time at different temperatures. The solid lines are the convolution of two exponentials fit to the data by least-squares fitting.

(C) The rate constants that determined the lag period in GroEL-GroES dynamics (k in Equation 2) and GFP folding (k in Equation 1) at three temperatures.

Bulk Phase Experiments Showed that FRET between Substrate Protein and GroEL Underwent Two Transitions after an Initial Rapid Change

As described above, GFP undergoes a ~3 s folding-arrested state in the initial *cis* ternary complex. To investigate whether this effect is specific for GFP or common to all substrate proteins, similar measurements for other substrate proteins should be performed. However, at present, rapid monitoring of the activity recovery of substrate protein in the *cis* ternary complex has been possible only for GFP, both for bulk phase experiment or single molecule imaging, due to technical difficulties. Instead of activity recovery, we performed ensemble measurement of the changes in fluorescence resonance energy transfer (FRET) between a substrate protein and the apical domain of GroEL (Figure 4A) as the transition of substrate protein from folding-arrested state to folding-competent state should accompany rearrangement of substrate protein in the *cis* ternary complex.

At first, the ensemble of FRET behavior of Cy3-labeled GFP was examined. The Cy3-GFP retained folding ability but recovered GFP fluorescence did not interfere with FRET measurement. A mutant GroEL, in which Glu315 at the apical domain was replaced with Cys (termed EL315) (Rye et al., 1999), was used for the specific labeling of an acceptor dye, IC5. EL315 and IC5-EL315 retained normal ATPase and chaperone activities of GroEL (data not shown). Cy3-GFP was denatured by 0.1 M HCl and diluted into a buffer containing IC5-EL315 to form a complex of Cy3-GFP and IC5-EL315. Then the fluorescence intensity of Cy3-GFP in the presence of EL315 with or without IC5 label was measured by a spectrometer to determine the efficiency of FRET. Upon formation of the complex Cy3-GFP and IC5-EL315, fluorescence intensity of the donor per acceptor decreased to 39% of that in the absence of acceptors, reflecting the close proximity of two dyes.

The GroEL cycle was initiated in the presence and absence of GroES by addition of ATP to the preformed Cy3-GFP-IC5-EL315 complex. In the absence of GroES, fluorescence intensity of the donor increased exponentially at a rate constant 0.13 s^{-1}, reflecting the simple release of Cy3-GFP from IC5-EL315. In the presence of GroES, by contrast, fluorescence intensity of the donor changed in three phases. An initial rapid increase transiently slowed, then increased again. The time course was simulated by assuming three rate constants, 2.1, 0.33, and 0.30 s^{-1} (Figure 4B). The first rate constant may represent a rapid transition that is included in the ~3 s lag. The second may represent the same transition that we observed as a lag in GFP folding. The third may correspond to the release of GFP into bulk solution.

Next, similar experiments were performed using MDH, a stringent substrate protein that folds efficiently only in the presence of GroEL, GroES, and ATP (Peralta et al., 1994; Chen et al., 2001). MDH was labeled with donor dye and Bodipy FL, and the labeled MDH (FL-MDH) retained the ability to fold within GroEL. FL-MDH was denatured in 6.4 M urea and diluted into the buffer containing IC5-EL315 to form a complex. Upon formation of the FL-MDH-IC5-EL315 complex, the fluorescence intensity of the donor per acceptor decreased to 51% of that in the absence of acceptors. The functional GroEL cycle was initiated by addition of ATP to the preformed

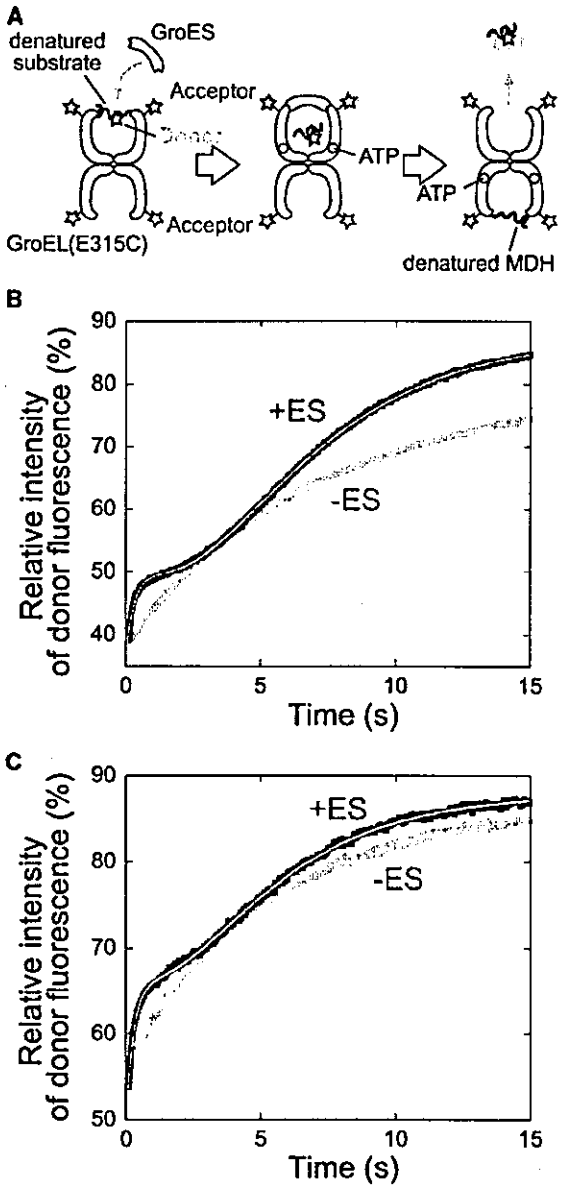

Figure 4. Bulk Phase Measurement of FRET between a Nonnative Protein and the Apical Domain of GroEL

(A) Schematic illustration of the FRET experiment. Denatured substrate protein with donor dye was trapped by EL315 with acceptor dyes. The functional GroEL cycle was initiated by addition of GroES, ATP, and excess nonlabeled denatured MDH to prevent rebinding of labeled denatured protein to EL315.

(B and C) Ensemble of the time course of the relative fluorescence intensity of (B) Cy3-GFP or (C) FL-MDH in the presence or absence of GroES. It was obtained from the ratio of the fluorescence of donor in the presence or absence of acceptor. The data were fit by assuming three-step reactions. Solid lines are the following functions. $D_4 + (D_1 - D_4)\exp(-k_1t) + (D_2 - D_4)k_1/(k_1 - k_2)[\exp(-k_2t) - \exp(-k_1t)] + (D_3 - D_4)k_1k_2/(k_1 - k_2)/(k_2 - k_3)/(k_1 - k_3)[(k_2 - k_3)\exp(-k_1t) - (k_1 - k_3)\exp(-k_2t) + (k_1 - k_2)\exp(-k_3t)]$. Parameters k_1, k_2, and k_3 are rate constants of a three-step reaction. D_1, D_2, D_3, and D_4 are percentages of donor fluorescence intensity.

FL-MDH-IC5-EL315 complex and GroES. The fluorescence intensity of the donor increased exponentially with a rate constant of 0.19 s^{-1} in the absence of GroES. In the presence of GroES, however, the intensity changed in three phases described by three rate constants, 2.9, 0.46, and 0.31 s^{-1} (Figure 4B). We also carried out experiments using Cy3-labeled MDH and obtained the three rate constants very similar to those with FL-MDH (data not shown). These results are similar to those obtained for the Cy3-GFP and indicate that the substrate protein-GroEL interaction changes in a characteristic manner, including a step that would be corresponding to the ~3 s lag observed in GFP folding kinetics.

Bulk Phase Experiments Showed that ATP Hydrolysis and Pi Release Are Described by the First Rate Constant and ADP Release by the Second Rate Constant

The results shown so far argue that the functional GroEL cycle proceeds with two major rate constants under optimum conditions. Since the whole cycle is driven by ATP hydrolysis, these two rate constants should correlate with the steps in ATPase cycle of GroEL. Although a number of studies on ATPase kinetics of GroEL and GroEL-GroES have been reported, all of these focused on ATPase activity in the absence of nonnative substrate protein (e.g., Todd et al., 1994; Cliff et al., 1999). Consequently, we performed ensemble measurements of the initial pre-steady-state time course of the ATPase cycle of GroEL in the presence of GroES and nonnative proteins. We employed three different assays (Figure 5A) to investigate each stage of the ATPase cycle. Hydrolytic cleavage of a β-γ bond of ATP was measured by total Pi generation with the malachite green method after the reaction was quenched by acid (Geladopoulos et al., 1991). This actually represents the progress of hydrolysis of GroEL-bound ATP. The release of Pi from GroEL was monitored by the Pi binding protein that captured free Pi in the medium and emitted enhanced fluorescence (Brune et al., 1994). Finally, release of ADP from GroEL was monitored by the appearance of free ADP in the medium by the oxidation of NADH with ATP regenerating auxiliary enzymes, pyruvate kinase, and lactate dehydrogenase (Pullman et al., 1960).

The results of total Pi generation are shown in Figure 5B. In the absence of GroES, Pi generation proceeded linearly with a single rate constant of 0.18 s^{-1} (gray line), but, in the presence of GroES, Pi generation started with an initial burst and reached a steady-state turnover (0.12 s^{-1}). The time course is consistent with Equation 3.

$$\begin{array}{c}[\text{ES-EL-ATP}]\rightarrow[\text{ES-EL-ADP-Pi}]\rightarrow \\ \qquad\quad k \qquad\qquad k' \\ [\text{ES}]+[\text{EL}]+[\text{ADP}]+[\text{Pi}]\end{array} \qquad (3)$$

The ATPase cycle has two steps with characteristic rate constants. ATP hydrolysis accompanies the first step. The solid line in Figure 5B is a simulated time course of the two rate constants, k = 0.31 s^{-1} and k' = 0.16 s^{-1}.

Similar to total Pi generation, Pi release from GroEL showed an initial burst in the presence of GroES and denatured MDH (Figure 5C). The time course of Pi release was simulated by Equation 4.

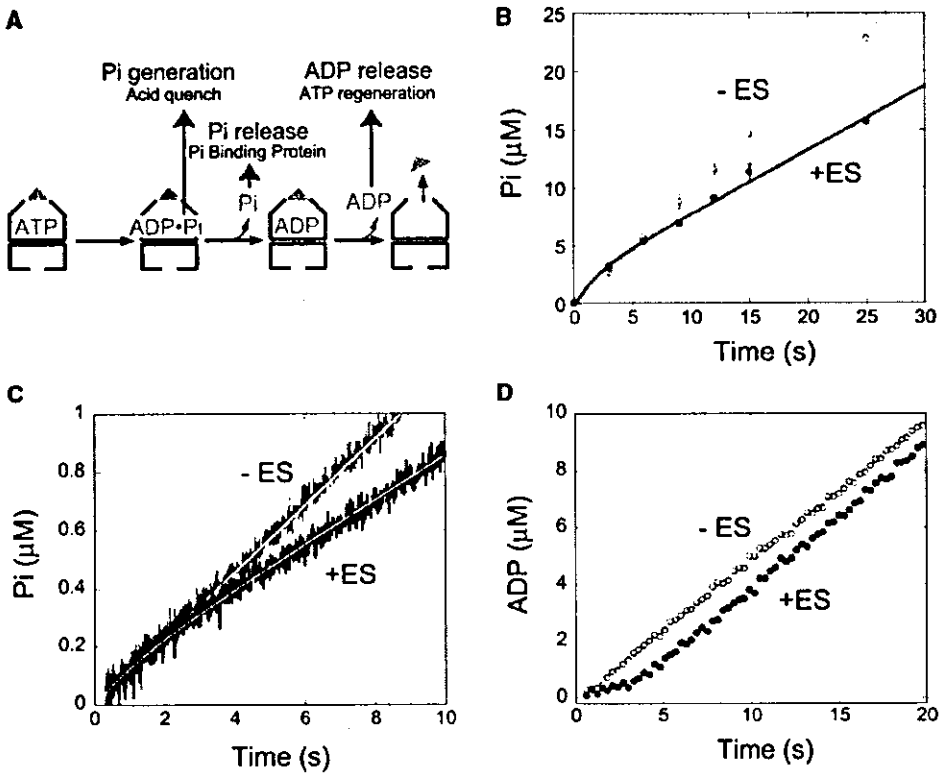

Figure 5. Bulk Phase Measurement of Initial ATPase Kinetics by GroEL in the Presence of Substrate Protein

(A) Schematic illustration of the three assays for ATP hydrolysis by GroEL: Pi generation, PI release, and ADP release.

(B) Ensemble of the time course of ATP hydrolysis by GroEL in the presence (closed circles) or absence (open circles) of GroES.

(C) Ensemble of the time course of Pi release from GroEL in the presence (black line) or absence (gray line) of GroES.

(D) Ensemble of the time course of ADP release in the presence (black line) or absence (gray line) of GroES. The solid lines fit to the data obtained in the presence of GroES are functions $C_1k\,(k't - k/(k + k')\,\{\exp[-(k + k')t] - 1\})/(k + k')$ in (B) and (C), and $C_2 + k\,k'/(k + k')\,(t + \exp[-(k + k')t]/(k + k')$ in (D). These formulas are derived from the two-step reaction of Equations 3 and 4. The solid lines fit to the data obtained in the absence of GroES are linear functions of C_3k t.

$$\underset{k}{\text{[ES-EL-ATP]}\rightarrow}\underset{k'}{\text{[ES-EL-ADP] + [Pi]}\rightarrow}$$

$$\text{[ES] + [EL] + [ADP] + [Pi]} \qquad (4)$$

There are two rate constants, k = 0.33 s^{-1} and k' = 0.37 s^{-1}, and Pi release takes place during the first step defined by k. Using pepsin and reduced α lactalbumin as substrate proteins, we carried out similar experiments and obtained the values k = 0.36, 0.26 s^{-1} and k' = 0.46, 0.20 s^{-1}, respectively. In the absence of GroES, on the other hand, no burst was observed and the ATPase cycle was defined by a single rate constant of 0.18 s^{-1}. The similarity of the k value for total Pi generation and that for Pi release suggests that Pi leaves GroEL immediately after Pi is generated by ATP hydrolysis on GroEL.

The time course of ADP release from GroEL in the presence of GroES and denatured MDH showed the initial lag and then reached the steady-state rate (0.12 s^{-1}) (Figure 5D). The time course was consistent with Equation 4. Two rate constants were calculated as k = 0.39 s^{-1} and k' = 0.23 s^{-1}, and ADP release occurred at the second transition defined by k'. Without GroES, ADP release proceeded linearly with time. Therefore, one product of ATP hydrolysis, ADP, stays bound for ~4 s after ATP hydrolysis until the next transition in the cycle completes while the other, Pi, leaves GroEL immediately after ATP hydrolysis.

Collectively, the data show that the ATPase cycle of GroEL proceeds with two major rate constants. The first ranges from 0.31 to 0.39 s^{-1} and defines both ATP hydrolysis on GroEL and Pi release from GroEL. The second ranges from 0.16 to 0.37 s^{-1} and governs the ADP release from GroEL. The values of the first rate constant are in close agreement with k values obtained from GFP folding and GroES release. This suggests that the same transition with this rate constant is responsible for the lags of GFP folding, GroES release, and ADP release and for the initial burst of ATP hydrolysis and Pi release. The second rate constants obtained from the ATPase cycle vary but are still in an acceptable range to suggest that they correspond to the rate constants k' obtained from other measurements.

Discussion

Two Timer Mechanism of the Functional GroEL Cycle

The single timer model of the functional GroEL cycle predicts that any events in the cycle after the *cis*-ATP

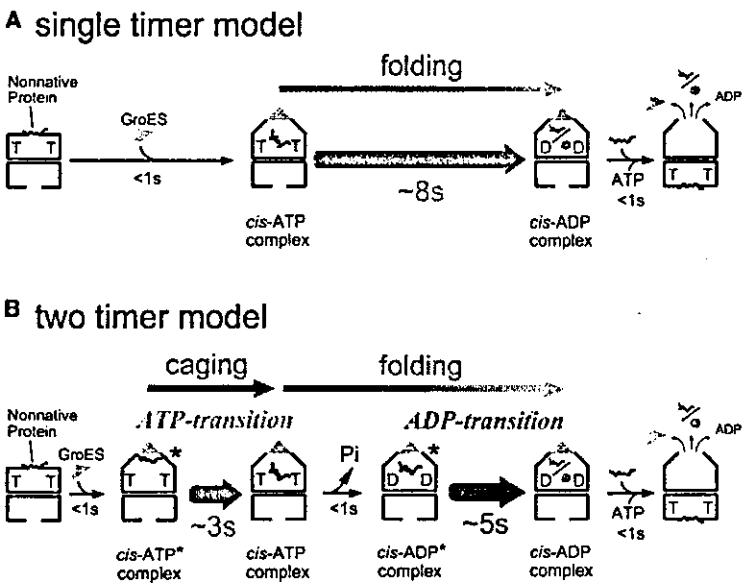

Figure 6. Single Timer Model and Two Timer Model of the Functional GroEL Cycle

(A) Single timer model of GroEL-GroES (Rye et al., 1999). In the presence of saturating amounts of ATP, GroES, and substrate proteins, only a single rate constant governs all events of the functional GroEL cycle, including ATP hydrolysis, release of Pi, ADP, GroES, and substrate protein from GroEL.

(B) Two timer model (this paper). In the presence of saturating amount of ATP, GroES, and substrate proteins, the functional GroEL cycle has two rate-limiting steps, which are represented by arrows colored red and blue. Binding of GroES (gray triangle) to the complex of GroEL-ATP-substrate protein produces the *cis*-ATP* complex in which substrate protein (green) is not fully released into the cavity. The first timer (lifetime, 3 s) is the "ATP transition" from the *cis*-ATP* complex to the *cis*-ATP complex, which results in full release of nonnative protein into the cavity where folding starts. ATP hydrolysis and Pi release of the *cis*-ATP complex occur rapidly to produce the *cis*-ADP* complex. The second timer (lifetime, 5 s) is the ADP transition from the *cis*-ADP* complex to the *cis*-ADP complex. The *cis*-ADP complex can accept ATP to the *trans* GroEL ring that induces rapid decay of the *cis* ternary complex (Rye et al., 1999). Encapsulation (caging) of the substrate protein occurs during ATP transition. Folding occurs in the *cis*-ATP complex and *cis*-ADP* complex.

complex should occur apparently with a single rate constant ~0.12 s^{-1} (lifetime, 8 s) (Figure 6A). This rate constant would correspond to the rate of ATP hydrolysis in the *cis* ring to produce the *cis*-ADP complex, the only rate-limiting step of the whole cycle (Weissman et al., 1996; Rye et al., 1997, 1999). However, all of the results in this report suggest that at least two rate-limiting steps exist in the cycle, and we propose here a model for the functional GroEL cycle, a successive two timer mechanism (Figure 6B). In this model, the GroEL-substrate protein complex binds ATP and GroES to generate the *cis*-ATP* complex in which, different from the *cis*-ATP complex in the single timer model, folding of substrate protein is arrested. The *cis*-ATP* complex is transformed to the *cis*-ATP complex with a rate constant ~0.3 s^{-1} (lifetime, 3 s). As soon as this transition takes place, three events immediately follow: the substrate protein becomes folding competent in the *cis* cavity, ATP is hydrolyzed, and Pi is released. The lifetime of the *cis*-ATP complex is very short, but folding continues in the next *cis*-ADP* complex. The *cis*-ADP* complex is further transformed to the *cis*-ADP complex with a rate constant ~0.2 s^{-1} (lifetime, 5 s). Similar to the *cis*-ADP complex in the single timer model, the *cis*-ADP complex in the two timer model can accept ATP and substrate protein to its *trans* ring, which immediately induces the decay of the *cis* ternary complex, that is, release of GroES, substrate protein, and ADP from the *cis* ring.

The ATP Transition Occurs without ATP Hydrolysis

The two timer mechanism assumes two critical transitions, from the *cis*-ATP* complex to the *cis*-ATP complex (ATP transition) and from the *cis*-ADP* complex to the *cis*-ADP complex (ADP transition) (Figure 6B). To define the ATP transition, it is important to note that an ATPase-deficient mutant EL398 (Figure 2C) or EL398/490 (Figure 1C) can mediate a single round *cis* folding of GFP with the same kinetics, ~3 s lag, as the EL490. This implies that nonnative GFP in the *cis*-ATP* complex reaches a folding-competent state prior to ATP hydrolysis. Therefore, the first rate-limiting step is not ATP hydrolysis. Rather, it is the conformational transition of the *cis*-ATP* complex that accompanies rearrangement of substrate protein from the folding-arrested state to the folding-competent state.

Rearrangement of Substrate Protein during the ATP Transition

The rearrangement of substrate protein in the complex during this transition was detected by FRET between substrate protein and GroEL (Figure 4). After a rapid increase that was not detected by other methods, the donor fluorescence increased with two transitions. The first likely reflects rearrangement of the substrate protein in the ATP transition and the second the decay of the *cis* ternary complex. The FRET time course of GFP and that of MDH are very similar. Likewise, the release kinetics of GroES in the functional GroEL cycle are not affected significantly by the species of substrate protein used: reduced α lactalbumin, an artificial nonstructured protein RP3-42, denatured pepsin, and denatured MDH (Taguchi et al., 2001). It appears that the timer is set only in the presence of substrate protein but ticks independent of the species of the bound substrate proteins. This was assumed in the single timer model, and it is also valid in the two timer model.

Horwich and his colleagues utilized fluorescence anisotropy of pyrene-labeled rhodanese and of intrinsic Trp of Rubisco to probe the rearrangement of substrate protein in the functional GroEL cycle initiated by addition of ATP and GroES to the GroEL-substrate protein complex (Weissman et al., 1996; Rye et al., 1997). For both substrates, two-phase transitions were observed, the first being a sharp drop in anisotropy (half time 1 s =

lifetime 1.4 s) reflecting the change of substrate protein from the restricted state to the flexible state (Weissman et al., 1996; Rye et al., 1997). The researchers assigned the flexible state to the folding-competent state in the *cis*-ATP complex but did not integrate the restricted state in their single timer model. However, we think that the most reasonable candidate for the restricted state might be the folding-arrested state in the *cis*-ATP* complex. The difference of lifetimes, ~1.5 s in their experiment and ~3 s in our model, is significant but acceptable when taking into account differing experimental conditions. Hydrogen exchange of substrate protein during functional GroEL cycle suggested a possible mechanical unfolding step before complete release of substrate protein into the *cis* cavity (Shtilerman et al., 1999). There is a possibility that this step might correspond to the *cis*-ATP* complex, but the short lifetime of this step (<1 s) makes this possibility rather unlikely. In addition, since another report using the same technique did not detect such an unfolding step (Chen et al., 2001), it is not clear that mechanical unfolding is a general step for various substrate proteins.

The Two Timer Mechanism Explains the Burst and Lag in the Initial Kinetics

Initial kinetics of ATP hydrolysis, GFP folding, and release kinetics of GroES in the cycle showed either lag or burst. We showed that upon initiation of the functional GroEL cycle by ATP addition, ATP hydrolysis in the *cis* ring, and release of Pi occurred as an initial burst with rate constant ~0.3 s^{-1} (Figures 5B and 5C). One might think from Figure 6B that there should be a lag rather than a burst for these events, because they occur after an event that has a lifetime of ~3 s. However, in general, if a rapid event follows a first slow event, these two events should be observed as if they occur simultaneously with the same rate constant, and a lag should not be observed in the rapid event. That happened in the case of ATP hydrolysis and Pi release, which occurred apparently at the same rate as that for ATP transition. Because the steady-state rate of ATP hydrolysis and Pi release (0.12 s^{-1}) is much slower than the initial rate (0.3 s^{-1}) due to the presence of the second rate-limiting step (0.2 s^{-1}), an initial burst should appear in the pre-steady-state kinetics. On the other hand, if a second slow event follows the first slow event, the second appears to occur after the lag period that corresponds to the time needed for the completion of the first slow event. This was the case for GFP folding, which showed a ~3 s lag. Following similar reasoning, decay of the *cis*-ADP complex (release of ADP, GroES, and substrate protein from GroEL) should be observed as if it occurs simultaneously with the ADP transition. Therefore, initial time courses of ADP release from GroEL showed a ~3 s lag when the cycle was initiated by addition of ATP.

The *cis*-ATP* Complex Ensures Efficient Caging of Substrate Protein

The essence of chaperonin function is encapsulation of nonnative protein into a narrow cage to facilitate folding in a protected environment (Weissman et al., 1995; Mayhew et al., 1996; Xu et al., 1997; Sakikawa et al., 1999). However, the mechanism of this efficient caging is only poorly understood. According to the single timer model, upon formation of the *cis*-ATP complex, GroES deprives the previously bound substrate protein of common binding sites on GroEL, and the substrate protein is released into the *cis* cavity. In a microscopic view, GroES can bind to GroEL only when nonnative substrate protein is released from GroEL to make the common binding sites available. It is unclear, however, how the release of substrate protein always results in encapsulation into the *cis* cavity rather than diffusing away to the bulk solution. The two timer model can offer rational explanation for the caging of the substrate protein. In the *cis*-ATP* complex, GroES is already bound but nonnative substrate protein remains in the folding-arrested state. This means that the polypeptide chain of the substrate protein should be interacting with the wall of the *cis* cavity. The ATP transition brings about a conformational change and the next intermediate, the *cis*-ATP complex, disfavors the interaction with substrate protein (Chaudhry et al., 2003). The substrate protein is thus set free to the *cis* cavity to start folding. Therefore the *cis*-ATP* complex plays a critical role in caging the substrate protein into the *cis* cavity.

The structural features of the *cis*-ATP* complex are as yet unknown. Intriguingly, the GroEL mutant C138W forms a folding-arrested *cis* ternary complex at 25°C, which can resume the cycle at 37°C (Kawata et al., 1999; Miyazaki et al., 2002). The arrested *cis* ternary complex of this mutant displays features of the *cis*-ATP* complex. It is noteworthy that substrate protein is located in a protease-inaccessible area in this complex. Amino acid residue C138 resides in the intermediate domain of GroEL and introduction of a bulky tryptophan at this position may restrict the hinge motion. One of candidates for the *cis*-ATP* complex could be such a complex in which a hinge of each GroEL subunit is partially "open."

Substrate Protein Is Free to Fold in the *cis*-ADP* Complex

It is well established that the substrate protein in the *cis*-ADP complex is released to the medium rapidly when ATP and nonnative substrate protein are present in the medium (Rye et al., 1999; Taguchi et al., 2001). Therefore, if the next intermediate after the *cis*-ATP complex is the *cis*-ADP complex, nonnative protein has little time to fold in the *cis* cavity. For this reason, a *cis*-ADP* complex, in which nonnative protein can fold, should be present before the *cis*-ADP complex. Our results show that the lifetime of the *cis*-ADP* complex, that is, the mean time given to nonnative protein to fold, is ~5 s. Because these two ADP complexes differ as to whether the *trans* ring can accept ATP or not, the ADP transition may bring about the conformational change mainly in the *trans* ring region. Cryo-electron micrography shows that the largest structural difference between the ATP-containing and ADP-containing GroEL-GroES complex is in the *trans* ring (Rye et al., 1999). This is reminiscent of the difference between *cis*-ADP* and *cis*-ADP complexes.

Both the ATP transition and the ADP transition do not accompany the change of chemical components of the complex. It seems that they are purely conformational

relaxation and that GroEL is at first raised to the "activated state" when it forms the *cis*-ATP* complex, and subsequent relaxation processes are coupled to exertion of the work. If this really is the case, the timers of GroEL are intrinsic ones built within the conformational dynamics.

Experimental Procedures

Proteins and Reagents

Bovine serum albumin, pepsin, glucose oxidase and catalase, "bacterial" purine nucleoside phosphorylase, phosphoenolpyruvate, and 7-methylguanosine were obtained from Sigma. Streptavidin and [2-(1-maleimidyl)ethyl]-7-(diethylamino)-coumarin-3-carboxamide (MDCC) were from Molecular Probes. Porcine heart malate dehydrogenase, rabbit muscle pyruvate kinase, and hog muscle lactate dehydrogenase were from Roche. The GroEL mutants (EL490, EL398, EL398/490, EL315) were produced by site-directed mutagenesis using the Kunkel method. GroEL mutants, GroES and GFP (S65T), were expressed in *Escherichia coli* and purified as described (Makino et al., 1997; Sakikawa et al., 1999; Motojima et al., 2000). GFP (S65T) was used throughout this work. Protein concentrations were determined by absorption spectroscopy using the following extinction coefficients at 280 nm: GroEL mutants 14-mer, 130480 $M^{-1}cm^{-1}$; GroES 7-mer, 8960 $M^{-1}cm^{-1}$; GFP (S65T) monomer, 18850 $M^{-1}cm^{-1}$. Protein concentration was expressed as oligomer (GroEL, 14-mer; SR1, 7-mer; GroES, 7-mer) throughout the study.

Microscopy

Total internal reflection fluorescence microscopy (TIRFM) was used for visualizing individual fluorescent molecules immobilized on the surface of a quartz slide. Single protein molecules labeled with Cy3 or IC5 were illuminated with a green solid-state laser (2.8 mW, 532 nm, μ-green model 4601, Uniphase, USA) or a He-Ne laser (1.0 mW, 632.8 nm, NEC, Japan), respectively. GFP molecules were illuminated with a blue solid-state laser (1.8 mW, 473 nm, HK-5511, Shimadzu Corporation, Japan) to visualize individual molecules. Images were taken by a SIT camera (C2400-08, Hamamatsu Photonics, Japan) coupled to an image intensifier (VS4-1845, Video Scope International, USA) and recorded on videotapes for subsequent analysis.

Imaging of GFP Folding

Folding of individual GFP molecules in GroEL was visualized by TIRFM. Both EL490 and EL398/490 were labeled with IC5-maleimide and biotin-$PEAC_5$-maleimide (Dojindo Laboratories, Japan) in buffer A (25 mM HEPES-KOH [pH 7.4], 100 mM KCl, 5 mM $MgCl_2$) as descrived previously (Taguchi et al., 2001). GFP (54 μM) was denatured for 2 min at 23°C in 0.1 M HCl and diluted to 2 μM with buffer A containing 400 nM EL490. After 5 min, EL490-denatured GFP complexes were infused into a flow cell and attached to the glass surface via streptavidin as described (Taguchi et al., 2001). Then the cell was filled with buffer A containing 1 μM GroES, 1 mM caged ATP, 25 units/ml apyrase, and an oxygen scavenger system (25 mM glucose, 2.5 μM glucose oxidase, 10 nM catalase, 10 mM dithiothreitol). The specimen was illuminated with a He-Ne laser to mark the position of EL490 and illuminated with a blue solid-state laser to visualize fluorescence of GFP. ATP was released by epifluorescence illumination of UV light for 250 ms with a 100 W mercury light source (U-MWU & IX-FLA, Olympus). Approximately 40% of caged ATP was split under the experimental condition, and ATP was hydrolyzed by apyrase in ~1 s. Appearance of the fluorescence of GFP at the position of EL490 after the photolysis of caged ATP was visualized by TIRFM. About 30% of the EL490 particles thus immobilized were active in folding of GFP.

Bulk Phase GFP Folding

In 1.2 ml of buffer A containing 5 mM dithiothreitol, 150 nM GroEL (EL490, EL398, or SR1), and 1.5 μM GroES at 23°C, 3 μl of acid-denatured GFP was diluted to a final concentration of 100 nM. After 15 min, 3 μl of ATP solution was added to a final concentration of 0.45 mM to start GroEL-GroES-assisted GFP folding. Fluorescence intensity of GFP was monitored continuously with a fluorometer (Ex 485 nm/Em 512 nm, F-4500, HITACHI). Dead time for the measurement was about 0.4 s.

Single Molecule Imaging of GroES-GroEL Dynamics

Single molecule imaging of GroEL-GroES dynamics was carried out using TIRFM as described (Taguchi et al., 2001). Experiments were performed at 18°C, 23°C, and 28°C.

Bulk Phase Measurements of FRET between GroEL and Substrate Protein

EL315 was labeled with IC5-maleimide. The molar ratio of IC5-label to the single ring of GroEL was 1.4. GFP was labeled with Cy3-NHS (Amersham-Pharmacia) at a molar ratio of 0.36. MDH was labeled with BodipyFL-SE (Molecular Probes) at a molar ratio of 0.25 per monomer. Cy3-GFP (8.3 μM) was denatured in 0.1 M HCl for 3 min and diluted to a final concentration of 50 nM with buffer A containing 100 nM IC5-EL315 and 5 mM DTT to make the complex of Cy3-GFP and IC5-EL315. After 5 min at 23°C, 3 μM GroES was added. The solution was loaded into a stopped-flow syringe, and buffer A containing 2 mM ATP, 5 mM DTT, and 1 μM denatured MDH was loaded into another syringe. Equal amounts of these solutions were mixed rapidly in a stopped-flow apparatus (RX 2000, Applied Photo Physics, UK) installed in a fluorometer (FP-6500, JASCO, Japan). The dead time for the measurement was about 0.07 s. To detect the fluorescence of Cy3 as a donor, the solution was excited at wavelength of 540 nm and the fluorescence from 565 to 575 nm was collected. A similar experiment was performed using EL315 without IC5 labeling. A time course of the relative intensity of Cy3 fluorescence was obtained from the ratio of Cy3-GFP fluorescence in the presence or absence of IC5-EL315 divided by the labeling ratio of IC5 per single ring of EL315. Förster distances between a Cy3-IC5 pair were expected to be ~4.9 nm (Wu and Brand, 1994). FRET between FL-MDH and IC-EL315 was measured as follows. FL-MDH (2 μM) was denatured in 6.4 M urea for more than 30 min at 23°C. Then it was diluted to the final concentration of 50 nM with buffer A containing 100 nM EL315, 5 mM DTT, and 3 μM GroES. Rapid mixing was performed as described for Cy3-GFP. The sample was excited at wavelength of 475 nm, and fluorescence from 507.5 to 512.5 nm was collected. Förster distances between a Bodipy FL-IC5 pair were expected to be ~4.7 nm.

Bulk Phase Measurements of Pre-Steady-State Kinetics of ATP Hydrolysis

The ATP hydrolysis reaction in the functional GroEL cycle was measured by three different assays at 23°C. Concentrations of the reaction components were varied to adjust the level suitable for each assay method.

Pi Generation

Generation of Pi from GroEL was measured using the malachite green assay (Geladopoulos et al., 1991). MDH (86 μM) denatured in 6 M urea was diluted to 3 μM into buffer A containing 1.5 μM GroEL and 5 mM DTT in the presence or absence of 4.5 μM GroES. After 5 min, 35 μl of the solution was injected into the same volume of buffer A containing 0.4 mM ATP that was vigorously stirred. The reactions were terminated by the addition of perchloric acid at the indicated times. The solution was centrifuged to remove protein precipitates. The supernatant was treated with a malachite green reagent, and the absorbance at 630 nm was measured.

Pi Release

Release of Pi from GroEL was measured using Pi binding protein (PBP) (Brune et al., 1994, 1998; Cliff et al., 1999). PBP labeled with MDCC, a coumarin derivative, was prepared as previously described (Brune et al., 1994, 1998). Binding of Pi to MDCC-labeled PBP (MDCC-PBP) increased the fluorescence emission at 466 nm when the complex was excited at 430 nm. By virtue of rapid binding of Pi to MDCC-PBP ($k_{on} = 1.36 \times 10^8\ M^{-1}\ s^{-1}$) and high affinity of PBP for Pi (K_d = 0.1 μM) (Brune et al., 1994, 1998), the increase in the Pi concentration in the solutions could be monitored as the increase of fluorescence emission in real time. To 1.2 ml of buffer A containing 0.07 μM GroEL, 10 μM MDCC-PBP in the presence or absence of 0.57 μM GroES, 12 μl of 60 μM MDH denatured in 6 M urea were added. After a 5 min incubation at 23°C, the solution was vigorously stirred and the reaction was initiated by injection of 1.5 μl ATP